Journal of Rare Earths 36 (2018) 165–169

Contents lists available at ScienceDirect

Journal of Rare Earths

journal homepage: http://www.journals.elsevier.com/journal-of-rare-earths

Structure and hard magnetic properties of $TbCu_7$-type $SmFe_{8.95-x}Ga_{0.26}Nb_x$ nitrides

Wenlong Yan [a], Ningtao Quan [a], Yang Luo [a, *], Dunbo Yu [a], Zilong Wang [a], Guiyong Wu [a], Kun Zhang [b]

[a] National Engineering Research Center for Rare Earth Materials, General Research Institute for Nonferrous Metals, and Grirem Advanced Materials Co., Ltd., Beijing 100088, China
[b] Key Laboratory of Microgravity (National Microgravity Laboratory), Institute of Mechanics, Chinese Academy of Sciences, Beijing 100190, China

ARTICLE INFO

Article history:
Received 27 July 2017
Received in revised form
31 October 2017
Accepted 1 November 2017
Available online 20 December 2017

Keywords:
Rapid-quenching
$SmFe_{8.95-x}Ga_{0.26}Nb_x$ alloy
$TbCu_7$-type structure
Magnetic properties

ABSTRACT

Nanocrystalline $SmFe_{8.95-x}Ga_{0.26}Nb_xN_\delta$ (x = 0, 0.1, 0.2, 0.3) were prepared using rapid-quenching, annealing and nitriding. The magnetic properties and crystal structures were systematically studied under various wheel velocities to investigate the influence of Nb doping for the compounds. It is found that $TbCu_7$-type structure is able to be obtained even though the wheel velocity is reduced to 20 m/s (x = 0.3). An significant increase (ΔT_c = 70 °C) of the Curie temperature is obtained with Nb doping at x = 0.1 due to the lattice expansion revealed by Rietveld analysis. The optimum coercivity with the value H_{cj} of 810 kA/m is achieved at x = 0.2 in the nitrides, in which a reasonable distribution of grain sizes of both $TbCu_7$-type $SmFe_9N_\delta$ and α-Fe can be found. However, an excess of Nb doping may lead to the increase of the weight fraction of α-Fe, which in turn deteriorates the magnetic properties.

1. Introduction

Since Coey et al.[1] discovered intermetallic compounds $Sm_2Fe_{17}N_x$, a systematical and profound study about them has been conducted. About one year later, Katter et al.[2] first discovered hexagonal $TbCu_7$-type phase in melt spun ribbons of binary Sm–Fe system. Stoichiometry of the $TbCu_7$-type phase is about $SmFe_9$, which has moderate coercivity upto 2.13 kOe. However, the $TbCu_7$-type phase is a meta-stable phase, and only at high cooling speed it can be obtained. In order to enhance and stabilize the magnetic properties, material researchers have already made some successful attempts by substitution of 3d and boron elements for iron.[3–7] The additional 3d element can facilitate $TbCu_7$-type structure and improve magnetic properties, such as V, Ti, Zr, Co, Al.[8–13] Recently, Our group[14] reported that the moderate doping content of Ga for $SmFe_9N_x$ compounds with $TbCu_7$-type structure was very effective to increase Curie temperature T_c and coercivity. However, the problem is that obtaining a single $TbCu_7$ phase still requires high velocity (50 m/s) and the magnetic property is relatively low.

This work is proposed to reduce the wheel velocity of obtaining a single $TbCu_7$ structure by adding Nb and further improve the magnetic properties as well based on the results mentioned above. Single phase materials of $SmFe_{8.95-x}Ga_{0.26}Nb_x$ were prepared, and the effects of Nb addition on the crystal structure, Curie temperature and hard magnetic properties were studied in the Nb doping $TbCu_7$-type Sm–Fe–Ga nitrides.

2. Experimental

$SmFe_{8.95-x}Ga_{0.26}Nb_x$ (x = 0, 0.1, 0.2, 0.3) parent alloys were prepared by induction melting Sm (99.9%), Fe (99.9%), Ga (99.9%) and Nb (99.9%) in Ar gas atmosphere. An extra amount of 25 wt% Sm was added to compensate the weight losses during melt-spinning and induction melting process. The molten ingots were ejected through an orifice of 0.7 mm in diameter at the bottom of a quartz crucible. All ribbons were prepared by melt spinning onto a rotating Cu-disk at a wheel speed of velocities 20–50 m/s (intervals 10 m/s). Subsequently, the ribbons wrapped in tantalum-foil were annealed at 800 °C for 1 h in vacuum ($<1.0 \times 10^{-3}$ Pa) and rapidly quenched with room temperature water. Then the annealed $SmFe_{8.95-x}Ga_{0.26}Nb_x$ powders were nitrided at 450 °C for 16 h in nitrogen atmosphere. The crystal structures and phases in the specimens were examined by X-ray diffraction (XRD) using Co Kα radiation by continuous (2θ = 0.02°, 20°–90°) and step mode (2θ = 0.02°, 20°–110°, counting time 4 s, 9 kW). The data were

* Corresponding author.
E-mail address: eluoyang@foxmail.com (Y. Luo).

https://doi.org/10.1016/j.jre.2017.11.001
1002-0721/

processed by Rietveld refinement with Rigaku Plus software. The thermomagnetic curves of the samples were tested using a vibrating sample magnetometer (VSM, Quantum Design VersaLab) with an applied field of 1000 Oe. Magnetic powder properties were measured at room temperature using a VSM in fields up to 3T. Microstructures of as-annealed ribbons were observed by transmission electron microscopy (TEM).

3. Results and discussion

3.1. Structure and phase analysis

Fig. 1 shows some X-ray diffraction patterns for $SmFe_{8.95-x}Ga_{0.26}Nb_x$ (x = 0, 0.1, 0.2, 0.3) alloys quenched at various wheel velocities of 20–50 m/s (interval = 10). It has been shown that the magnetic phases are obvious changed, depending on the Nb content and the speed of rapid-quenching velocities. For $SmFe_{8.95-x}Ga_{0.26}Nb_x$ (x = 0) alloy, the single $TbCu_7$-type structure was able to be obtained when the speed of velocities reach to 50 m/s. However, when the speed of velocities is lower than 50 m/s, the main phase is the rhombohedral Th_2Zn_{17}-type structure with a small amount of $SmFe_2$ and α-Fe phases which is from Fig. 1(a). With the content of Nb increasing, the lowest speed of velocities to obtain single $TbCu_7$-type structure gradually decreased as shown in Fig. 1. Furthermore, the single $TbCu_7$-type structure was able to be obtained even though the speed of velocities was 20 m/s with Nb doping at x = 0.3, which can be seen from Fig. 1(d). The reason can be attributed to the increasing undercooling of $SmFe_{8.95-x}Ga_{0.26}Nb_x$ alloys by adding high melting point metal Nb, which can impel the formation of the $TbCu_7$-type structure in the melt spun Sm–Fe alloys. However, an excess of Nb doping may lead to the increased content of α-Fe and precipitation of the Nb_2Fe_7 phase with main $TbCu_7$-type phase, which in turn deteriorates the magnetic properties, which is in agreement with the literature that[8] the independence of formation of the $TbCu_7$-type phase on the wheel velocities in the range of 15–50 m/s for the melt spun $Sm_{10}Fe_{82.5}V_{7.5}$ alloys, due to the substitution effect of vanadium for iron, can impel the formation of the $TbCu_7$-type structure in the melt spun Sm–Fe alloys. As a result, we concluded that the magnetic phases are sensitively dependent both on the composition and the wheel velocity and the $TbCu_7$-type phase shows a tendency to form in higher wheel speed, which is different from the situation of the Th_2Zn_{17}-type structure.[15]

The crystal structure of the as-annealed ribbons has been refined by Rietveld method based on the $TbCu_7$-type structure. The observed patterns agree well with the final calculated patterns. The results are shown in Table 1, which illustrates the variation of lattice parameters and axial ratio c/a value with the content of Nb element (v = 40 m/s). With the increase of Nb doping ($x \leq 0.2$), the lattice parameter a decreases and the c increases, as a result, a greater expansion of c/a value is observed. In general, the main phase of $TbCu_7$-type structure tends to form in the compounds when the c/a value dropped in the range of 0.8499–0.8699, which is in agreement with the that of Katter et al.[2] And the greater the ratio of c/a is, the more stable the $TbCu_7$-type crystal structure will be.[7,16] On the contrary, an excessive doping of Nb (x = 0.3) can lead to a decline in c/a, corresponding to a trend of instability for $TbCu_7$ structure.

Table 1
Lattice parameters, grain size of the ribbons from the Rietveld refinement and T_c for as-annealed $SmFe_{8.95-x}Ga_{0.26}Nb_x$ ribbons.

	x = 0	x = 0.1	x = 0.2	x = 0.3
a/nm	0.4925	0.4917	0.4916	0.4911
c/nm	0.4228	0.4265	0.4266	0.4243
c/a	0.858	0.867	0.868	0.864
T_c/K	470	540	420	410
d/nm	62	37	32	30

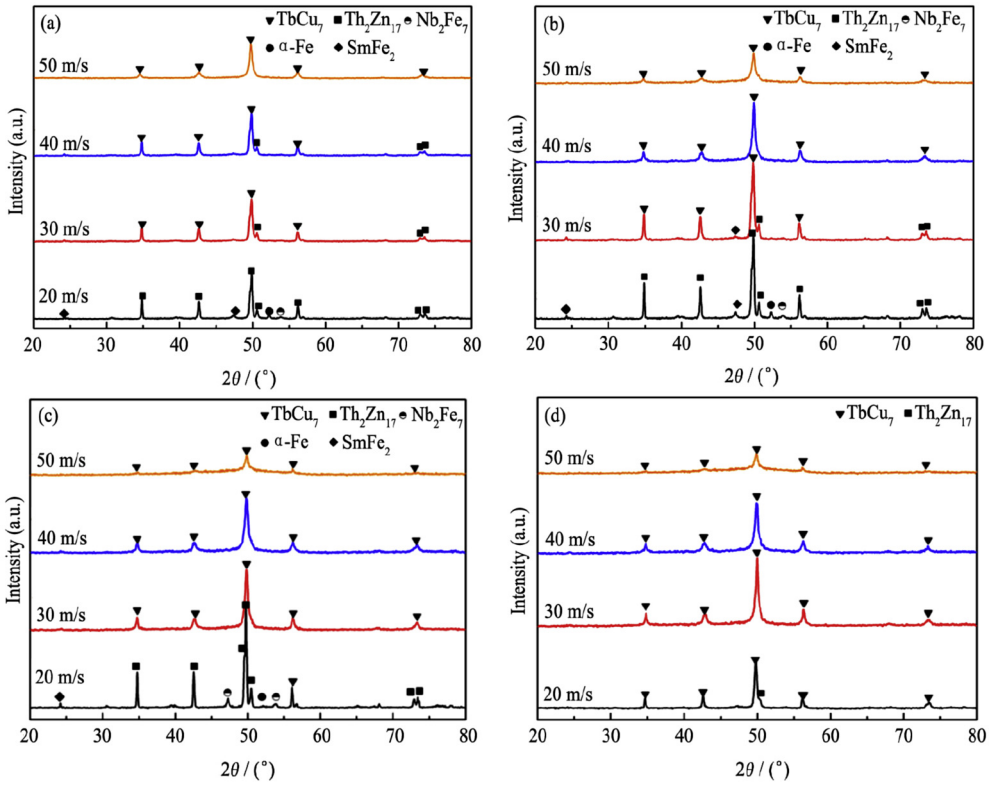

Fig. 1. X-ray diffraction patterns of as-annealed $SmFe_{8.95-x}Ga_{0.26}Nb_x$ (x = 0 (a), 0.1 (b), 0.2 (c), 0.3 (d)) ribbons prepared at various wheel velocities of 20–50 m/s.

Fig. 2 shows thermomagnetic behaviors for as-annealed ribbons in a magnetic field of 1000 Oe (v = 40 m/s). Remarkably, the Curie temperature of the as-annealed $SmFe_{8.95-x}Ga_{0.26}Nb_x$ ribbons increases from 470 K for x = 0–540 K for x = 0.1. To certify it, the average iron moment $<\mu_{Fe}>$ for each compound is calculated at the dumbbell sites from the saturated moments, based on the hypothesis that an opposing magnetic moment of each samarium is equal to 0.90 μ_B.[17] It can be found that $<\mu_{Fe}>$ increases slightly from 1.66 μ_B for x = 0–1.72 μ_B with Nb doping of x = 0.1 shown in Fig. 3. It can be attributed to the enhanced Fe–Fe interaction, which is consistent with increase of the Curie temperature. Furthermore, the Curie temperatures of 540 K for $SmFe_{8.95-x}Ga_{0.26}Nb_x$ (x = 0.1) is much higher than that of $SmFe_{12}$,[18–20] or Sm_5Fe_{17} based alloys[21] previously reported.

3.2. Nitrogenation and magnetic properties

Nitrides of $SmFe_{8.95-x}Ga_{0.26}Nb_x$ (x = 0, 0.1, 0.2, 0.3) alloys were obtained by quenching at 40 m/s, crystallization annealing at 800 °C for 60 min in vacuum (<1.0 × 10^{-3} Pa) and subsequent nitriding at 450 °C for 16 h in nitrogen atmosphere. Fig. 4 shows the hysteresis loop of the nitride powders of $SmFe_{8.95-x}Ga_{0.26}Nb_x$ (x = 0, 0.1, 0.2, 0.3), which were measured in an maximum applied field of ±30 kOe. The greatest magnetic property of B_r = 0.76 T, H_{cj} = 810 kA/m, and $(BH)_{max}$ = 80 kJ/m^3 was obtained in the nitride powders of $SmFe_{8.95-x}Ga_{0.26}Nb_x$ ribbons at x = 0.2. Magnetic energy product has been improved by 32 kJ/m^3 and the intrinsic coercivity increased by 320 kA/m compared to Nb-free.[12] It can be seen that the demagnetization curve "step" become smaller, which means the increase of magnetic performance. This can be explained from two aspects. On the one hand, the maximum c/a ratio is obtained for x = 0.2, which can improve the efficiency of nitriding, and the maximum c/a ratio increases interstitial lattice of 3f site occupied by N atoms, according to Teresiak et al.[22] Fig. 5(a) shows XRD patterns of $SmFe_{8.75}Ga_{0.26}Nb_{0.2}$ alloys with different conditions treatment in order to investigate the structure after nitriding, The diffraction peaks of as-annealed Sm–Fe alloys are similar to that of as-quenched sample. But the diffraction peaks of the nitrides shift toward the left because N atoms penetrate into the gap of crystal lattice. Fig. 5(b) shows the thermomagnetic behaviors for as-annealed and nitridation of $SmFe_{8.95-x}Ga_{0.26}Nb_{0.2}$

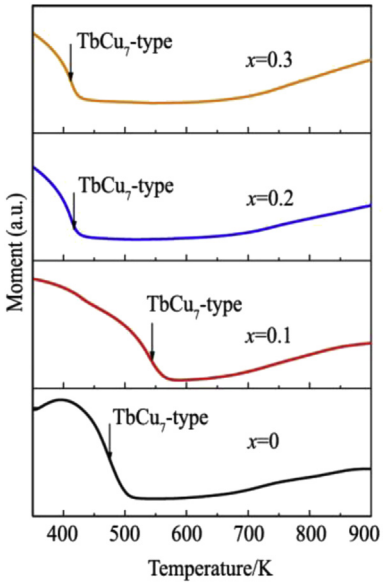

Fig. 2. Thermomagnetic behavior of as-annealed $SmFe_{8.95-x}Ga_{0.26}Nb_x$ (x = 0, 0.1, 0.2, 0.3) ribbons with $TbCu_7$-type structure (40 m/s).

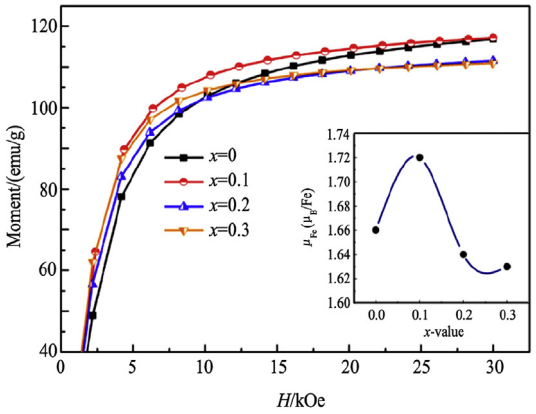

Fig. 3. The initial magnetization curves for as-annealed $SmFe_{8.95-x}Ga_{0.26}Nb_x$ (x = 0, 0.1, 0.2, 0.3) ribbons at 25 °C. Inset shows $<\mu_{Fe}>$ as a function of Nb content.

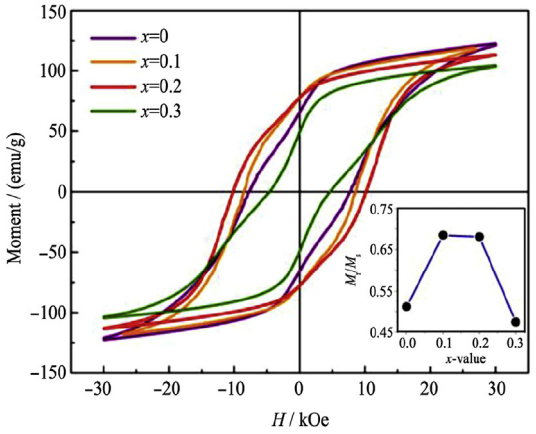

Fig. 4. Hysteresis loop of $SmFe_{8.95-x}Ga_{0.26}Nb_xN_\delta$ powders. Inset shows the change of M_r/M_s.

alloys in a magnetic field of 1000 Oe. The Curie temperature of the as-annealed $SmFe_{8.95-x}Ga_{0.26}Nb_{0.2}$ ribbons increases from 420 K for x = 0–750 K after nitriding.

On the other hand, the microstructure of the as-annealed $SmFe_{8.75}Ga_{0.26}Nb_{0.2}$ ribbons is more homogeneous than that of Nb-free ribbons according to Fig. 6(b). Furthermore, we can see the grain size of nitridation $SmFe_{8.95-x}Ga_{0.26}Nb_x$ (x = 0.2) has not changed in Fig. 6(c). The grain size of $SmFe_{8.75}Ga_{0.26}Nb_{0.2}$ ribbons is about 35 nm, much smaller than the grain size (62 nm) of Nb-free

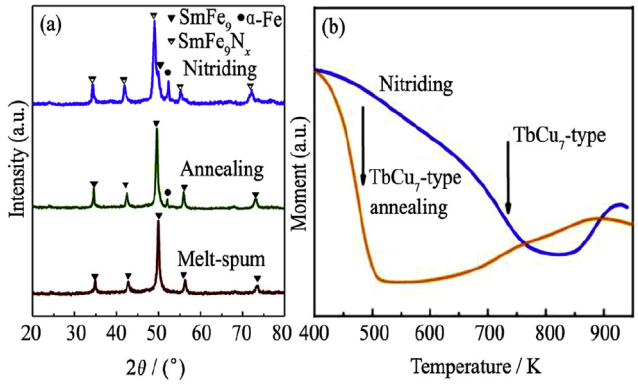

Fig. 5. X-ray diffraction patterns of melt spun, annealed and nitridied of $SmFe_{8.75}Ga_{0.26}Nb_{0.2}$ powders (a), and the thermomagnetic behavior of annealed and nitridated $SmFe_{8.75}Ga_{0.26}Nb_{0.2}$ powders (b).

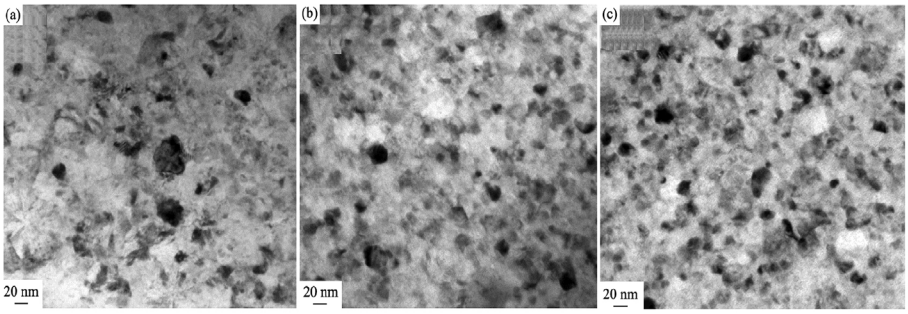

Fig. 6. TEM micrographs of as-annealed $SmFe_{8.95}Ga_{0.26}$ (a), micrographs of as-annealed $SmFe_{8.75}Ga_{0.26}Nb_{0.2}$ (b) and TEM micrographs of $SmFe_{8.75}Ga_{0.26}Nb_{0.2}N_{\delta}$ (c).

ribbons, which is consistent with the Rietveld refinement as displayed in Table 1. However, the demagnetization curve in Fig. 4 ($x = 0.3$) shows up steep step, which results in the deterioration of the remanence as well as the coercivity, the reason is that excess doping of Nb ($x = 0.3$) can result in a slight decline in c/a and the increased contents of α-Fe as indicated from XRD Rietveld refinement results displayed in Table 2, which means a trend of instability for $TbCu_7$ structure.

A small amount of α-Fe emerges for each $SmFe_{8.95-x}Ga_{0.26}Nb_x$ compound as displayed in Table 2. Henkel plots for the $x = 0.2$ sample are selected to investigate intergranular exchange coupling existing in the $SmFe_{8.95-x}Ga_{0.26}Nb_xN_{\delta}$ compounds. The expression which is the interaction between soft magnetic phase and hard magnetic phase was given as follows[23]:

$$\delta_m(H) = [M_d(H) - M_r + 2M_r(H)]/M_r$$

Where the remanent magnetization $M_r(H)$ is acquired after the application and subsequent removal of direct field H, the remanent magnetization $M_d(H)$ after DC saturation in one direction and the subsequent application and removal of a direct field H in the reverse direction. Fig. 6 shows the henkel plots of the $SmFe_{8.75}Ga_{0.26}Nb_{0.2}N_{\delta}$ powders. Obviously, there is no exchange coupling indicated by the negative peak of δ_m which is observed in Fig. 7. The non-existing exchange coupling may be ascribed to the relatively larger grain size of α-Fe phase in the present work due to the relatively lower wheel velocity of 40 m/s. The grain size of α-Fe phase determined by the XRD Rietveld in Table 2 is approximately in nm, which is somewhat difficult to expect the hard magnetic properties by the exchange coupling phenomena.[24] It is in agreement with the report by Katter et al.[8] that the exchange coupling existing in the nanocomposite magnetic system was obtained in the higher wheel velocity of 60 m/s.

Table 2
Grain size of α-Fe phase in as-annealed $SmFe_{8.95-x}Ga_{0.26}Nb_x$ alloys obtained from the Rietveld refinement.

Composition	α-Fe grain size/nm	Content α-Fe/wt%
$x = 0$	50.1	7.3
$x = 0.1$	31.7	1.3
$x = 0.2$	30	0.72
$x = 0.3$	28.1	2.5

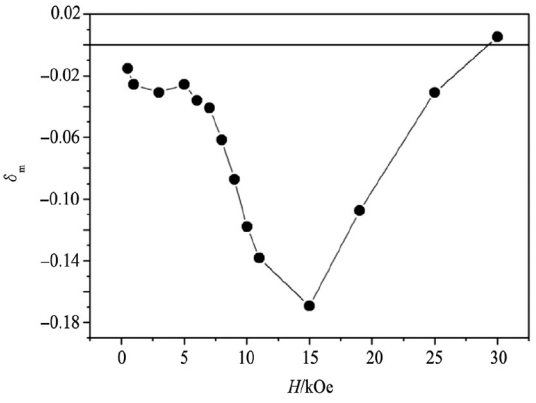

Fig. 7. The Henkel plots of the $SmFe_{8.75}Ga_{0.26}Nb_{0.2}N_{\delta}$ powders.

4. Conclusions

The crystal structures and hard magnetic properties of melt-spun $SmFe_{8.95-x}Ga_{0.26}Nb_x$ ribbons and their nitrides were studied to illustrate the influence of Nb substitution for Fe in the compound. Firstly, the single $TbCu_7$-type structure is able to be obtained at the relatively low velocity of 20 m/s because of Nb doping ($x = 0.3$). Secondly, an significant increase ($\Delta T_c = 70$ °C) of the Curie temperature is obtained with Nb doping at $x = 0.1$ compared to the Nb-free samples. Thirdly, the optimum coercivity with the value H_{cj} of 810 kA/m is gained at $x = 0.2$ in the nitrides. Finally, an excess of Nb doping will deteriorate the magnetic properties instead, which may be ascribed to the increase of the weight fraction of α-Fe.

References

1. Coey JMD, Sun H. Improved magnetic properties by treatment of iron-based rare earth intermetallic compounds in ammonia. *J Magn Magn Mater*. 1990;87(3):L251.
2. Katter M, Wecker J, Schultz L. Structural and hard magnetic properties of rapidly solidified Sm-Fe-N. *J Appl Phys*. 1991;70(6):3188.
3. Sakurada S, Tsutai A, Hirai T, Yanagida Y, Sahashi M, Abe S, et al. Structural and magnetic properties of rapidly quenched $(R,Zr)(Fe,Co)_{10}N_x$ (R=Nd,Sm). *J Appl Phys*. 1996;79(8):4611.
4. Mochizuki M, Shimizu M, Murakawa M, Tanigawa S. Magnetic properties and crystal structures of nanocrystalline Sm-Fe-Co-Nb-B compounds. *J Jpn Soc Powder Powder Metall*. 2003;50(1):22.
5. Yamamoto H, Matsumoto S, Fukuno A. Magnetic properties of $TbCu_7$-type Sm-Fe-Co-Nb-Zr system nitriding compounds. *J Jpn Soc Powder Powder Metall*. 2001;48(2):184.
6. Zheng CJ, Yu DB, Li KS, Luo Y, Jin JL, Lu S, et al. Effect of boron additions on phase formation and magnetic properties of $TbCu_7$-type melt spun SmFe ribbons. *J Magn Magn Mater*. 2016;412:89.
7. Luo Y, Zhang K, Li KS, Yu DB, Jin JL, Men K. Structure and magnetic behaviors of melt-spun SmFeSiB ribbons and their nitrides. *J Magn Magn Mater*. 2016;405:214.
8. Suzuki S, Yamamoto H. Magnetic properties of melt-spun $Sm_{10}(Fe, V)_{90}Ny$ with $TbCu_7$-type structure. *IEEE Trans Magn*. 1995;31(1):902.
9. Gebel B, Kubis M, Müller KH. Permanent magnets prepared from $Sm_{10.5}Fe_{88.5}Zr_{1.0}N_y$ without homogenization. *J Magn Magn Mater*. 1997;174(1–2):L1.
10. Makridis SS, Tang W. Structural and magnetic properties of Sm $(Co_{0.7}Fe_{0.1-}Ni_{0.12}Zr_{0.04}B_{0.04})_{7.5}$ melt spun isotropic and anisotropic ribbons. *J Rare Earths*. 2012;20(7):691.
11. Shield JE, Li CP, Branagan DJ. Microstructures and phase formation in rapidly solidified Sm-Fe and Sm-Fe-Ti-C alloys. *J Magn Magn Mater*. 1998;188(3):353.
12. Yang FM, Li XW, Tang N, Wang JL, Lu ZH, Zhao TY, et al. Magnetic properties of $Sm_2Fe_{17}N_y$ with Al substituted for Fe. *J Alloys Compd*. 1995;221(1–2):248.
13. Luo Y, Yu DB, Li HW, Zhuang WD, Li KS, Mao YJ, et al. Structure and permanent magnetic properties of $SmFe_x$ (x=3–8) melt spun ribbons during heat treatment. *J Rare Earths*. 2014;32(10):960.

14. Quan NT, Zhang SR, Luo Y, Jin JL, Zhang K, Liu YC. Crystal structure and hard magnetic properties of $TbCu_7$-type $Sm_{0.98}Fe_{9.02-x}Ga_x$ nitrides. *J Rare Earths*. 2014;32(8):722.
15. Kim HT, Xiao QF, Zhang ZD, Geng Y, Kim YB, Kim TK, et al. Phases of melt-spun $Sm_{1-x}Fe_{7+x}$ alloys and magnetic properties of their nitrides. *J Magn Magn Mater*. 1997;173(3), 295.
16. Sun JB, Cui CX, Zhang Y, Li L, Gao JX, Liu YL. Structural and magnetic properties of $Sm_2Fe_{17-x}Nb_x$ (x=0–4) alloys prepared by HDDR processes and their nitrides. *Rare Met*. 2006;25(2):129.
17. Bessais L, Dorolti E, Djéga-Mariadassou C. Combined effect of gallium and carbon on the structure and magnetic properties of nanocrystalline $SmFe_9$. *J Phys Condens Matter*. 2006;18(15):3845.
18. Müller A. Magnetic material R, Fe, Mo, (Co) with $ThMn_{12}$ structure. *J Appl Phys*. 1988;64(1):249.
19. Mooij DBD, Buschow KHJ. Some novel ternary $ThMn_{12}$-type compounds. *Journal Commun Monogr*. 1988;136(2):207.
20. Hu J, Wang T, Zhang S, Wang Y, Wang Z. Structure and magnetic properties of $RTi_{1.1}Fe_{10.9}$. *J Magn Magn Mater*. 1988;74(1):22.
21. Stadelmaier HH, Schneider G, Henig ET, Ellner M. Magnetic $Fe_{17}R_5$ in the Fe-Nd and Fe (-Ti)-Sm systems, and other phases in Fe-Nd. *Mater Lett*. 1991;10(7–8):203.
22. Teresiak A, Kubis M, Mattern N, Wolf M, Gruner W, Müller KH. Influence of nitrogenation on structure development and magnetic properties of mechanically alloyed and annealed Sm–Fe powders. *J Alloys Compd*. 1999;292(1):212.
23. Kelly PE, Grady KO, Mayo PI, Chantrell RW. Switching mechanisms in cobalt-phosphorus thin films. *IEEE Trans Magn*. 1989;25(5):3881.
24. Schrefl T, Kronmüller H, Fidler J. Exchange hardening in nano-structured two-phase permanent magnets. *J Magn Magn Mater*. 1993;127(3):L273.